Numerical Simulation of Bed Variation in a Channel with a Series of Submerged Groins

T. Uchida[1] and S. Fukuoka[2]
Research and Development Initiative
Chuo University,
1-13-27 Kasuga, Bunkyo-ku, Tokyo, 112-8551
JAPAN
E-mail: [1] utida@tamacc.chuo-u.ac.jp, [2] sfuku@tamacc.chuo-u.ac.jp

Abstract: *A practical numerical bed variation method for evaluating various functions of groins in rivers is required. The 2D method is inadequate to simulate local scouring around structures due to 3D flow. On the other hand, full 3D turbulence methods are still limited for applications to floods in natural rivers. Therefore, a refined depth integrated method is required for the practical use. In this paper, the Bottom Velocity Computation (BVC) method is developed to evaluate velocity acting on sediment particles effectively. In the BVC method, depth-integrated horizontal vorticity and water surface velocity equations are computed simultaneously with shallow water equations. To compute bed variation around submerged groins, evaluation methods for non-equilibrium bed load and bed tractive force by using bottom velocity is adopted. The adequacy of the method is discussed through the comparisons with the laboratory experimental results in a channel with a series of submerged groins.*

Keywords: *A series of submerged groins, bottom velocity, horizontal vorticity, local scouring, non-equilibrium bed load, bed tractive force.*

1. INTRODUCTION

Groins have been installed for countermeasures against bed scouring and bank erosion, for formation of fairways and flood channels in rivers. Recently, the environmental functions as generating various bed topographies around groins are focused. On the other hand, it has been indicated that the installations of groins have a possibility of causing the other bed scouring problems (Fukuoka *et al.*, 2002). To install groins in rivers, it is necessary to understand not only local bed topography around a groin but also bed variation on a river scale, such as longitudinal bed profiles.

There are many previous researches on developing a practical bed variation analysis around groins. For example, Fukuoka *et al.* (1992, 1998, 2002) developed a quasi-three dimensional numerical method, which composed of equations for vertical velocity distribution with shallow water equations, to develop a practical bed variation analysis around groins. However, it is known that the previous quasi-three dimensional method is still-inadequate for local scouring induced by complex flows, such as horseshoe vortex in front of structures and flow separation behind structures, because they cannot consider effects of non-hydrostatic pressure distribution on vertical velocity distributions. The horseshoe vortex and local scouring around single non-submerged structure, such as a groin and a pier, have been calculated successfully by full 3D turbulence methods coupled with sediment transport models (e.g., Nagata *et al.*, 2005; Roulund *et al.*, 2005). McCoy *et al.* (2008) investigated flow and turbulence structures in a channel with a series of groins by LES. As indicated above, a full 3D turbulence method is becoming an important tool to clarify complex flow fields around structures. However, simulations by full 3D turbulence methods are still confined to spatial-temporal small scale phenomena of flow and bed variation. So, a practical and reliable method for flows and bed variations during floods are required.

Recently, to compute bed variation around a pier, Uchida & Fukuoka (2010) developed the Bottom Velocity Computation (BVC) method, which was composed of depth-integrated horizontal vorticity and water surface velocity equations in addition to shallow water equations. The objective of this study is to develop the Bottom Velocity Computation method for the evaluation of bed variation in a channel with a series of submerged groins. This paper presents evaluation methods for flow and vortex motion around submerged groins and evaluation methods for non-equilibrium bed load and bed tractive force by using bottom velocity. The adequacy of the method is discussed through the comparisons with the laboratory experimental results in a channel with a series of submerged groins.

2. COMPUTATION METHOD

2.1. Bottom Velocity Computation Method

Bottom velocity acting on sediment particle is important for many bed variation analyses. Uchida & Fukuoka (2010) developed the Bottom Velocity Computation (BVC) method to evaluate bottom velocity distributions without computing vertical distributions of velocity and pressure intensity, based on the depth integrated method with horizontal vorticity equations (Uchida & Fukuoka, 2009). Figure 1 shows the concept of Bottom Velocity Computation (BVC) method. We define the bottom z_b as the surface on the thin vortex layer δz_b on the bed. The velocity on the bottom velocity u_{bx} is the computation object of BVC method and represented by equation *(1)* for the shallow water condition (Uchida & Fukuoka, 2009, 2010):

$$u_{bx} = u_{sx} - \Omega_y h \tag{1}$$

where, u_{sx}: water surface velocity, Ω_y: depth-averaged vorticity, h: water depth. The equation *(1)* means that we can evaluate the bottom velocity u_{bx} by computing water surface velocity u_{sx}, depth-averaged horizontal vorticity Ω_y and water depth without computing vertical velocity and pressure distributions.

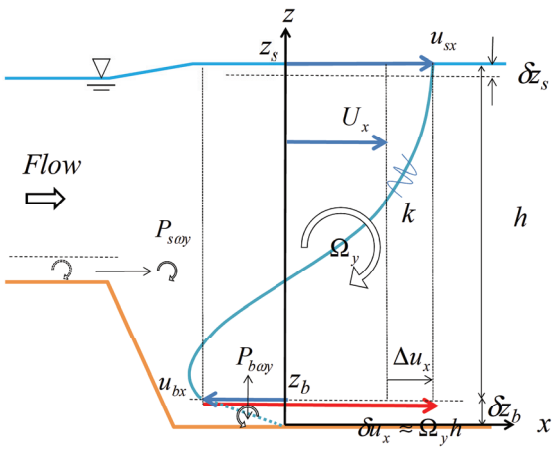

Figure 1 The concept of Bottom Velocity Computation method.

To evaluate bottom velocity by the equation *(1)*, BVC method is composed of depth-integrated horizontal vorticity equation *(2)* and water surface velocity equation *(3)* in addition to shallow water equations *(4)*,*(5)* and turbulence energy transport equation *(6)* (Uchida & Fukuoka, 2010).

$$\frac{\partial \Omega_i h}{\partial t} = ER_{\sigma i} + P_{\omega i} + \frac{\partial h D_{\omega ij}}{\partial x_j} \tag{2}$$

where,Ω_i: depth averaged horizontal vorticity in i direction, $ER_{\sigma i}$: rotation term of vertical vorticity, $P_{\omega i}$: production term of vorticity from the bottom thin vortex layer, $D_{\omega ij}$:: horizontal vorticity flux due to convection, rotation, dispersion and turbulence diffusion.

$$\frac{\partial u_{si}}{\partial t} + u_{sj}\frac{\partial u_{si}}{\partial x_j} = -g\frac{\partial z_s}{\partial x_i} + P_{si} \tag{3}$$

where, u_{si}: water surface velocity in i direction, g: gravity, z_s: water level, P_{si}: production term due to shearstress acting on thin water surface layer δz_s.

$$\frac{\partial h}{\partial t} + \frac{\partial U_j h}{\partial x_j} = 0 \tag{4}$$

$$\frac{\partial \rho U_i h}{\partial t} + \frac{\partial \rho U_i U_j h}{\partial x_j} = -\rho g h\frac{\partial z_s}{\partial x_i} - \tau_{0i} + f_i + \frac{\partial h \tau_{ij}}{\partial x_j} \tag{5}$$

where, U_i= depth averaged horizontal velocity in i direction, τ_{0i}: bed shear stress, τ_{ij}: horizontal shear stress due to turbulence and vertical velocity distribution.

$$\frac{\partial k}{\partial t} + U_j\frac{\partial k}{\partial x_j} = \frac{1}{h}\frac{\partial}{\partial x_i}\left(\frac{\nu h}{\sigma_k}\frac{\partial k}{\partial x_i}\right) + P_k - \varepsilon \tag{6}$$

where, k= depth averaged turbulence energy, P_k: production term, □: dissipation term. The terms in these equations are evaluated by the following vertical velocity distribution. By using depth averaged velocity U_i, velocity difference δu_i between water surface u_{si} and bed surface u_{bi} and no vertical velocity gradients on water surface, vertical velocity distribution of a cubic curve is obtained:

$$u_i = U_i + \Delta u_i\left(12\eta^3 - 12\eta^2 + 1\right) - \delta u_i\left(4\eta^3 - 3\eta^2\right) \tag{7}$$

where, $\Delta u_i=u_{si}-U_i$, $\delta u_i=u_{si}-u_{bi}$, $\eta=(z_s-z)/h$.

Submerged groins are inputted as the bed elevation, as shown in Figure 2. To evaluate the discontinuity of the bed elevations around groins by the depth integrated method, the following methods are adopted. The form drag acting on the submerged groin is evaluated by the external force term f_i in the momentum equations, following previous methods based on the depth integrated equations. The term f_i is evaluated by equation *(8)*, using the local pressure increment dp in front of the groin:

$$f_i = k\frac{\partial dp}{\partial x_i}, \quad dp = C_D\frac{\rho u_a^{\,2}}{2} \tag{8}$$

where, k: groin height, C_D: drag coefficient (C_D=1.0), u_a : approaching velocity as indicated in Figure 2. The vortex motion around the submerged groin is modelled as followings. The horseshoe vortex in front of the structure is developed by the vortex stretching of the approaching flow. In addition to the vortex stretching, the vorticity in front of the submerged groin is developed, because the strong vortex is trapped near the bed. In this method, vorticity flux over the groin are evaluated by the product of average vorticity and velocity from the groin top to the water surface, as shown in Figure 2. On the other hand, separation vortex is supplied to the flow from the back of the groin by Equation *(9)* of the production term in the vorticity equation.

$$P_{s\omega y}\Delta x = \left|u_{bx}/2\right| \cdot \left(-u_{bx}\right) \tag{9}$$

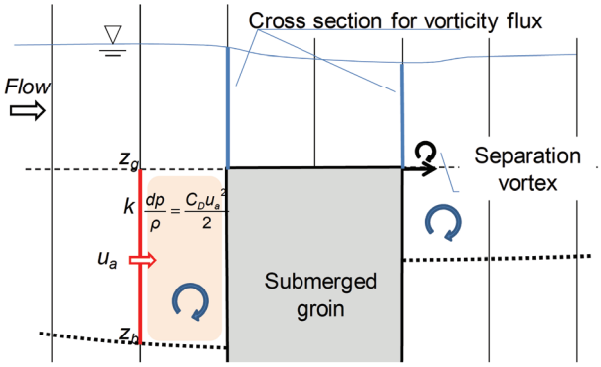

Figure 2 Evaluation method of flow and vortex motion around a submerged groin.

2.2. Bed Variation Computation Method

It is necessary to evaluate non-equilibrium sediment transport to compute the local scouring around the submerged groin, which is induced by the complex bottom velocity field with the horseshoe vortex in front of the structure and the separation vortex behind the structure as indicated in Figure 7. In this study, the bedload rate is computed by the following equation *(10)*, which was derived by the momentum equation for sediment (Uchida & Fukuoka, 2010).

$$\frac{\partial q_{Bi}}{\partial t} + \frac{\partial u_{Bj}q_{Bi}}{\partial x_j} = \left(Pu_{BPi} - Du_{BDi}\right) + m_* h_B\left(\gamma_{ei} - \gamma_i\right) \tag{10}$$

where, q_{Bi}: bedload sediment transport rate vector, u_{Bi}: sediment particle velocity vector of bedload, Pu_{BPi}: gain momentum from bed material, Du_{BDi}: loss momentum by particle deposition, $m_*=\mu_k sg\cos\theta/(s+1+C_M)$, C_M : coefficient of added mass, μ_k: dynamic friction coefficient of sediment, s: specific gravity of sediment in water, θ: bed gradient, $h_D=q_D/u_D$, $q_D^{\,2}=q_{Di}q_{Di}$, $u_D^{\,2}=u_{Di}u_{Di}$, γ_i, γ_{ei}: unit vector of sediment movement and that for the equilibrium condition. The above variables and coefficients are decided by the reference to previous researches on sediment transport as similar to Uchida & Fukuoka (2010).

The total resistance of bed is evaluated by Manning roughness coefficient n. The coefficient n for the total resistance is decided as presented in the following chapter 3.2. The total resistance of bed with sand waves is divided into form drag acting on sand waves and surface resistance acting on sediment particles. The latter is considered as bed tractive force. Generally, the surface resistance is evaluated by using equivalent roughness k_s of sediment particle. In this study, the surface resistance in non-equilibrium flow conditions is evaluated by the Boussinesq approximation near the bed (Uchida & Fukuoka, 2010). The bed tractive force and the critical shear stress of sediment particle on bed slope are given by Fukuoka & Yamasaka (1983). The equilibrium bed load is given by Ashida & Michiue (1974). And where the local bed slope exceeds the angle of repose, bed topography is modified by sand slide.

3. BED VARIATION ANALYSIS IN A CHANNEL WITH A SERIES OF SUBMERGED GROINS

3.1. Experimental Conditions

Fukuoka *et al*. (1998) presented experimental results for flow and bed variations in a channel with a series of submerged groins. The experiments were conducted in a straight channel, 1.5m width, 27.5m long with submerged groins, 0.5m length, 0.05m width and 0.03m initial height. Uniform bed material $d=0.80*10^{-3}$m were used. The submerged groins were installed along the left bank of the channel. Effects of groin angle to the main flow and longitudinal interval of groins on bed topography in a channel and local scouring around groins were examined. Constant sediment supplies were given at upstream end of the channel for each experimental case. In this paper, the method is applied to Experiment 2 (Fukuoka *et al*., 1998) which was conducted for the condition indicated in Table 1.

Table 1 Experimental Condition. (Experiment 2, Fukuoka *et al*., 1998)

Channel width	1.5 m
Channel length	27.5 m
Water Discharge Q	$36.4*10^{-3}$ m^3/s
Sediment Discharge Q_s	$4.0*10^{-6}$ m^3/s
Sediment diameter d	$0.80*10^{-3}$ m
Initial Bed Slope I	1/600
Groin Length D	0.50 m
Groin Width	0.05 m
Initial Groin Height k	0.03 m
Longitudinal Groins Interval L	1.0 m
Angle of groin	90°
Number of groins	15

3.2. Computational Conditions

The computational domain covers the whole experimental channel. The experimental water discharge Q and sediment discharge Q_s are given at the upstream of the domain. The computational water level at the downstream end of the domain is adjusted to reproduce measured water level at the downstream end. Manning roughness coefficient n for total bed resistance and coefficient C_{qB} of Ashida & Michiue formula (1974) are assumed temporally constant. The Manning roughness coefficient n is decided n=0.017 to reproduce the initial longitudinal water surface profile of Figure 3 by the computation. Then, sediment discharge coefficient C_{qB} is decided C_{qB}=9 to reproduce the temporal change in the longitudinal water surface profile of Figure 3 by the computation.

3.3. Longitudinal bed profiles and sediment discharge

Figure 3 shows comparisons of temporal changes in longitudinal water level and bed level between the measurement (Fukuoka *et al*., 1998) and the computation. In the measurement, the water surface slope is high at first, and then decreases due to degradation of bed level in the installation section of

groins. It is presented that the method is able to capture both temporal changes in longitudinal profiles of measured water levels and bed levels. Figure 4 shows comparisons of temporal changes in sediment discharge between the measurement (Fukuoka *et al.*, 1998) and the computation by present method. The measured sediment discharge is time-averaged value. The measured sediment discharge at channel downstream end is initially much larger than the sediment supply at upstream end, and then reduces asymptotically to the constant value. Because the measured sediment discharge is almost constant after 30 hours, this stage is regarded as the dynamic equilibrium stage of sediment motion. The computed sediment discharge at the channel downstream end at the dynamic equilibrium stage gives close agreement with that of the measurement. On the other hand, the measured sediment discharge at upstream of the groins installation section is initially almost zero, and then become asymptotically to the amount of the sediment supply soon after the first sand wave by the sediment supply reaches the section. The method shows a good explanation of reproduces temporal change in longitudinal bed profiles and sediment discharge.

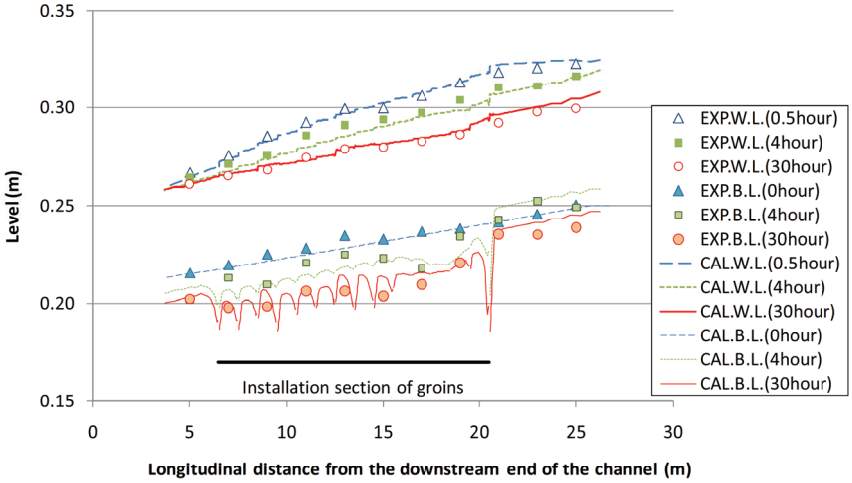

Figure 3 Comparisons of temporal changes in longitudinal water and bed level between the measurement (Fukuoka *et al.*, 1998) and the computation by present method.

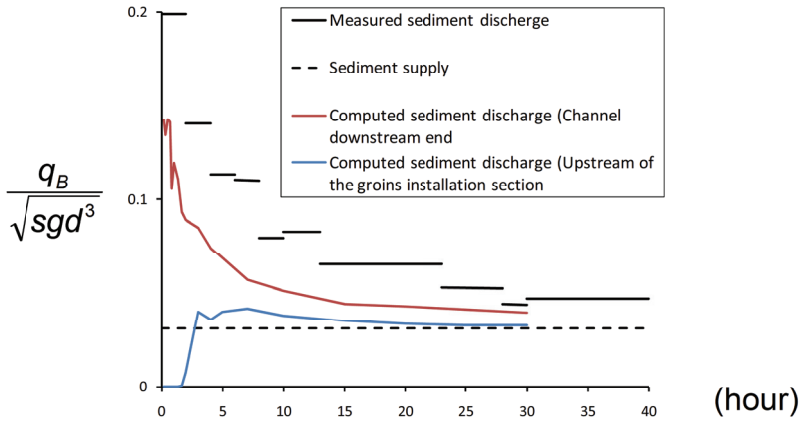

Figure 4 Comparisons of temporal changes in sediment discharge between the measurement (Fukuoka *et al.*, 1998) and the computation by present method.

3.4. Bottom velocity distribution and bed topography around groins in the midstream of the channel

Figure 5 shows computed bed topography in the channel at the dynamic equilibrium stage. For the upstream part in the installation sections of groins, the bed level of the main stream area degrades due to the flow concentration by the first groin (indicated Zone A in Figure 5). From the middle to the downstream of the installation sections, longitudinal bed degradation zone is created near the groin tip with local scouring (indicated Zone B in Figure 5). Figure 6 shows comparisons of bottom velocity distributions and bed topography at the dynamic equilibrium stage around the groins installed in the midstream (indicated Zone C in Figure 5) between (a) the measurement and (b) the computation. Figure 7 shows flow structures around a submerged groin. In front of the groin, horizontal vortex filaments in the approaching flow are convected and stretched, which induce the vorticity strengthening. And the vorticity near the bed is converged, because the intense vorticity near the bed hardly flows over the groin. The above induces inverse bottom flow in front of the groin. And the horseshoe vortex is induced around the tip of the groin, like the flow around a pier (e.g., Nagata *et al.*, 2005; Roulund *et al.*, 2005; Uchida & Fukuoka, 2010). The bottom velocity field by the above mechanism induces local scouring around groins, as indicated in Figure 6 (a). On the other hand, inverse bottom velocity is caused by the flow separation at the back of the groin and the low bottom velocity occurred between groins. The above induced the sediment deposition between groins, as indicated in Figure 6 (a).

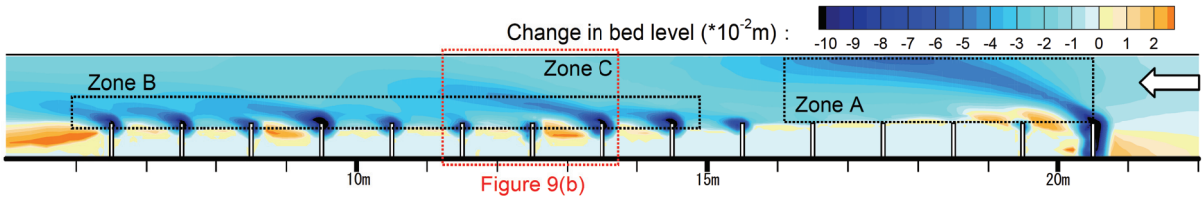

Figure 5 Computed bed topography in the channel at the dynamic equilibrium stage.

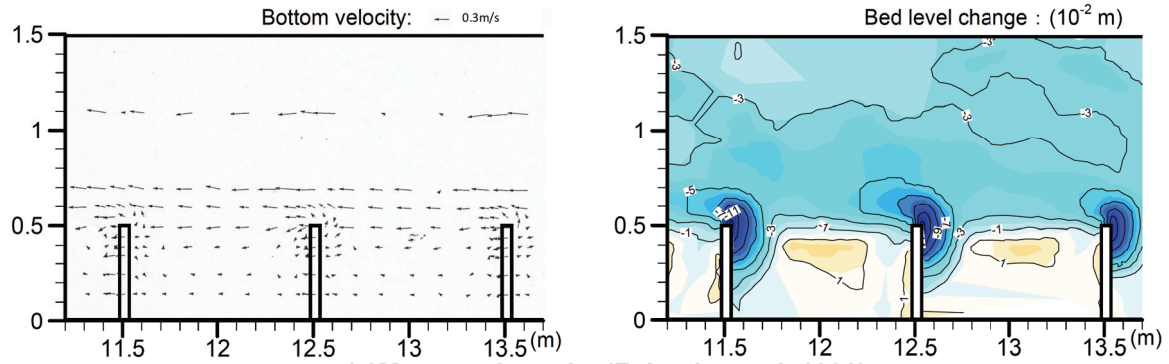

(a)Measured results (Fukuoka *et* al, 1998)

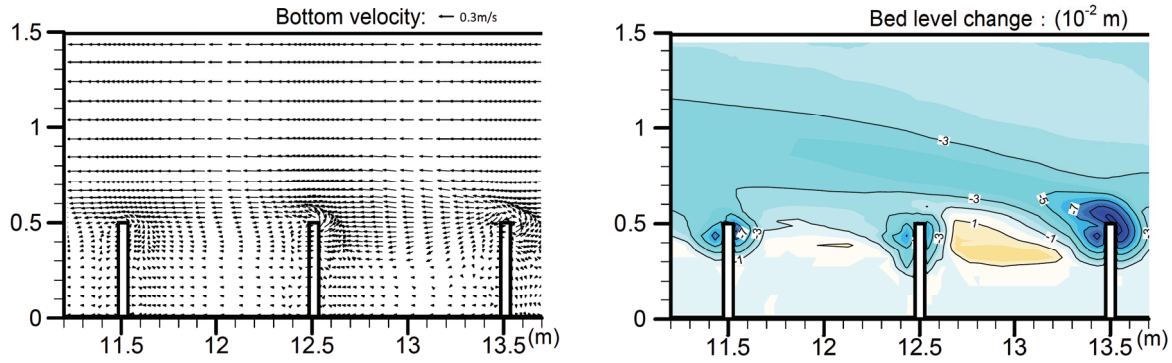

(b) Computed results

Figure 6 Bottom velocity distributions and bed topographies in the midstream of the installation section by the measurement and the computation at the dynamic equilibrium stage.

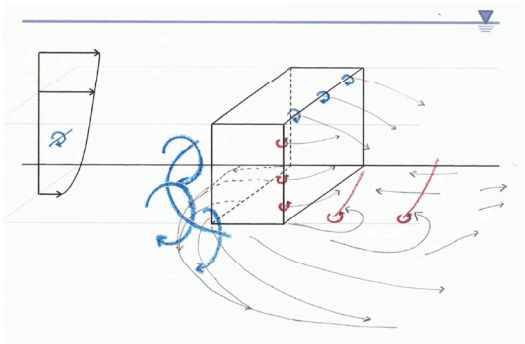

Figure 7 Flow structures around a submerged groin.

The method reproduces characteristics of measured bottom velocity field, such as horseshoe vortex in front of the groins, inversed bottom velocity at the back of the groin, and less bottom velocity between groins. Computed scour holes are a little smaller than measured holes. However, computed inverse flow of the tip of the groin is a little stronger than that of measurement, because of the assumption of equation (1). The above indicate the main reason of discrepancy of scour holes between computed and measured results is not attributed to bottom velocity computation but to bed variation computation. Specifically, sediment pick-up rate is considered to be underestimated, because the method is not account for the effects of turbulence and vertical velocity on sediment motion. This remains to be solved. However, it is considered that the computed bed topography explains the measured characteristics of scouring in front of the groins and deposition between of the groins.

3.5. Longitudinal distribution of maximum sour depth

Figure 8 shows a comparison of longitudinal distributions of maximum scour depth around groins obtained by the experiment and the computation. The maximum scour depth dz_{max} is nondimensionalized by the groin height k and the longitudinal distance x from the first groin is nondimensionalized by the groin length D. The scour hole around the first groin x/D=0 is deeper and larger than that of the other groins due to high approaching velocity. On the other hand, scour holes around groins installed within about 10 times distance of the groin length D downstream from the first groin (0<x/D<10) are not developed, because the first groin bends the approaching flow toward the right bank. For the downstream of the above groins (x/D>10), the maximum scour depth varies little longitudinally. The followings are comparisons between the experiment and the computation. The computed maximum scour depths are smaller than the measured depths. Especially for groins installed behind the first groin (0<x/D<10), there are little scour holes by the computation, although measured scours for 0<x/D<10 have the half depth of the first scour. And the longitudinal variation of the computed scour depth in the downstream part of the group (x/D>10) is relatively large compared with that of the measurement. These discrepancies are considered to be attributed to the present bed variation computation method, as discussed in the forgoing section. However, it is demonstrated that the present method can explain the characteristics of the longitudinal maximum scour depth distribution, such as large scour depth for x/D=0, undeveloped scour depth for 0<x/D<10 and recovered scour depth for x/D>10.

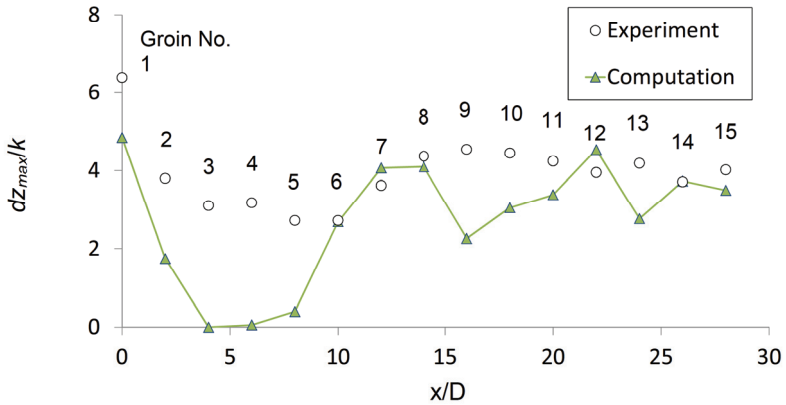

Figure 8 Longitudinal distribution of maximum scour depth around groins

4. CONCLUSIONS

The present paper develops the bottom velocity computation method and bed variation computation method in a channel with a series of submerged groins. The following conclusions are obtained by the comparisons with the experiment:

(1) The method reproduces temporal change in longitudinal bed profiles and sediment discharge.

(2) The method reproduces measured bottom velocity field around submerged groins, and computed bed topography explains the measured characteristics of scouring in front of the groins and deposition between the groins.

(3) The method reproduces the characteristics of the longitudinal maximum scour depth distribution.

5. REFERENCES

Ashida, K. and Michiue, M.(1972): *Study on hydraulic resistance and bed-load transport rate in alluvial stream*, Proceedings of the Japan Society of Civil Engineers, Vol.206, pp.59-69, in Japanese.

Fukuoka, S., Nishimura, T., Okanobu, M. and Kawaguchi, H.(1998), *Flow and bed topography around groins installed in a straight channel*, Annual Journal of Hydraulic Engineering, JSCE, Vol.42, pp.997-1002, in Japanese.

Fukuoka, S., Tsuchiya, S., Abe, T. and Nishimura, T.(2002), *Design of bed variation control measures at Ojiya – Koshiji district in the Shinano River,* Journal of Hydraulic, Coastal and Environmental Engineering, JSCE, No.698/II-58, pp.21-32, in Japanese.

Fukuoka, S. and Yamasaka, M.(1983), *Alternating bars in a straight channel*, Proceedings of the Japanese Conference on Hydraulics, JSCE, pp.703-708, in Japanese.

Fukuoka, S., Watanabe, A. and Nishimura, T.(1992), *On the groin arrangement in meandering rivers*, Journal of Hydraulic Engineering, JSCE, No.443/II-18, pp.27-36, in Japanese.

McCoy, A., Constantinescu, G. and Weber, L.J.(2008), *Numerical investigation of flow hydrodynamics in a channel with a series of groynes*, Journal of hydraulic engineering, ASCE, Vol.134, No. 2, pp.157-172.

Nagata, N., Hosoda, T., Nakato, T. and Muramoto, Y.(2005), *Three-dimensional numerical model for flow and bed deformation around river structures*, Journal of Hydraulic Engineering, ASCE, No.131, No.12, pp.1074-1087.

Roulund, A., Sumer, B.M., Fredsøe, J. and Michelsen, J.(2005) *Numerical and experimental investigation of flow and scour around a circular pile*, Journal of Fluid Mechanics, 534, pp.351-401.

Uchida, T. and Fukuoka, S. (2009) *A depth integrated model for 3D turbulence flows using shallow water equations and horizontal vorticity equations*, 33rd IAHR Congress: Water Engineering for a Sustainable Environment, pp.1428-1435.

Ushida, T. and Fukuoka, S. (2010), *Practical numerical simulation method for estimating local scouring around a pier: Bottom velocity computation method based on depth integrated model*, 11th International Symposium on River Sedimentation, ISRS, Stellenbosch, South Africa.